Experimental evaluation of indoor optical wireless MIMO systems with square and linear array constellations

Tetsuya Nakamura*, **Chedlia Ben Naila***, ***Member, IEEE***,
Kentaro Kobayashi†, ***Member, IEEE***, **Hiraku Okada***, ***Member , IEEE***,
Masaaki Katayama*, ***Senior Member, IEEE***
**Nagoya University, Nagoya 464-8603, Japan*
†*Meijo University, Nagoya 468-8502, Japan*

Abstract: In this paper, we investigate the performance of the newly designed 4×4 optical wireless multiple-input-multiple-output (MIMO-OWC) system based on a linearly-shaped arrangement of transmitters and receivers, to achieve long-distance and high data rate transmission. To highlight the importance of selecting an appropriate arrangement for the optical elements, we carried on a comparative study, considering both the conventional square and the proposed horizontal linear constellation of optical modems. The performance of the bit error rate (BER) is experimentally evaluated at distances up to 65 m, using two important metrics inherent to the MIMO transmission channel matrix, i.e., the Frobenius norm and the condition number. The results show that the channel matrix shape characterized by the condition number dominates the BER if the Frobenius norm is smaller than 1. Furthermore, the proposed MIMO-OWC system employing a linearly-shaped arrangement of transmitters and receivers, shows to be more immune to the calibration error rather than the conventional square constellation optical modems. Moreover, the transmission of 100 Mbps data-rate and a BER lower than 10^{-4} could be successfully achieved at a 65 m communication range.

Index Terms: Optical wireless communications, OWC, optical wireless MIMO, array constellations, Indoor wireless communications, Long distance communications.

1. Introduction

Connected Industries, firstly introduced by Society 5.0 initiative [1], is defining the upcoming generation of Smart Industry which is envisioned as an ambitious extension of Industry 4.0 [2]. This innovative concept is geared towards highly-automated, faster, more flexible, and smarter manufacturing processes. This rapid transformation into more customized and digitized production implies further stringent demands in terms of capacity, reliability, security, and low latency. To meet such challenges, the radio-frequency (RF) wireless technologies were extensively studied as possible candidates to consider.

However, the industrial indoor environment is particularly harsh to radio-frequency (RF) propagation due to the complex reflections and radio wave shielding caused by any large metal devices or products existing in the factory. Hence, the high-level generated electromagnetic noise may significantly degrade the system communication quality, restricting the use of RF-based technologies in industrial wireless applications [3], [4]. To overcome this impediment and fulfill the demanding requirements, optical wireless communications (OWC) technologies can be considered as a potential

alternative. OWC can offer better security at the physical layer thanks to the spatial confinement inherent to the optical carriers and enjoys the availability of unlicensed and interference-free optical spectrum. Therefore, the industrial networks, based mainly on wired connections so far, can migrate easily and quickly into hybrid solutions that incorporate RF as well as optical wireless links without the need to redesign the whole communication infrastructure [5].

Driven by the ever-increasing demand for higher capacity within the Connected Industries platform, different multiplexing methods, commonly used in both RF and optical fiber communication systems, have been investigated to design the most appropriate OWC system for such industrial applications. For instance, with the use of the very mature technique of wavelength division multiplexing (WDM), a high data rate of 4.5 Gbps [6] or 10 Gbps [7] could be achieved. In these studies, a transmitter based on a complex high-precision optical system design is considered. However, in indoor industrial environments, implementing high-speed OWC links with relatively simple optical LED-based system is desirable. Nonetheless, the light directivity and intensity of LEDs remain considerably inferior to the lasers, thereby making the realization of a high-speed transmission over a distance exceeding 10 m very challenging [8]. On the other hand, the use of another spatial multiplexing method which is the multiple-input-multiple-output (MIMO) approach, based on using multiple transmitters and receivers, has been shown to enhance significantly the capacity of OWC systems as reported in [9]–[12]. For instance, the transmission of very high data rate, namely 500 Mbps using 2×2 MIMO system [9] and 1 Gbps using 3×3 MIMO system [10], could only be achieved over a very short distance of 40 cm and 1 m, respectively. On the other hand, by applying a 4×4 MIMO system, a lower data rate of 16 Mbps [11] and 50 Mbps [12] was transmitted at a distance of 1 m and 2 m, respectively. In these previous research works, a high-speed transmission could only be achieved over short distances of a few meters. In order to further extend the communication range, our successful attempt to transmit a data rate of 20 Mbps at a distance of 15 m was firstly reported in [13]. Afterward, we could demonstrate to achieve the same data rate at a longer distance of 60 m [14].

Although the performance of the transmission channel matrix of MIMO-OWC systems depends closely on the arrangement of optical arrays of the transceivers, a little work has been done on clarifying and characterizing this relationship. For instance, the authors in [15] and [16], evaluated this impact and showed that the optical element arrangement affected the transmission. But, this numerical analysis was only carried over short distances, ranging from 3 m to 6 m. Moreover, the impact of the spacing of optical elements over long-distance communications exceeding 10 m has also been evaluated experimentally and numerically in [17] and [18], respectively. In [14], we proposed to use an improved design of the MIMO-OWC system that features a new one-dimensional arrangement of optical modulator array at both the transmitter and the receiver sides and evaluate its performance experimentally. Nonetheless, the use of different optical array constellations and their impact on the overall system performance had not been studied. Therefore, the main purpose of this research is to extend our previous work reported in [14] and elaborate a comparative study considering two different constellations of optical arrays, i.e., a new linear arrangement and the conventional two-dimensional one. The impact of the selection of the arrangement of optical arrays on MIMO-OWC system performance is characterized in terms of the channel matrix characteristics and the bit error rate (BER), over long distances.

2. System configuration

In this section, we present in details the new transceiver design featuring a linear arrangement of optical arrays instead of the conventional two-dimensional rectangular arrangement of array elements, as shown in Fig. 1.

2.1. Transmitter

Fig. 2 (a) illustrates the general configuration of the MIMO-OWC transmitter. The transmitter comprises two main units, namely a "Transmitter signal processor unit" and an "Optical Modulator

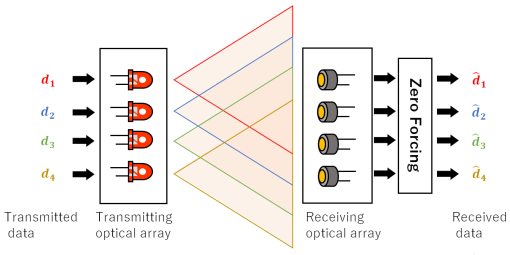

Fig. 1. Concept of MIMO-OWC system

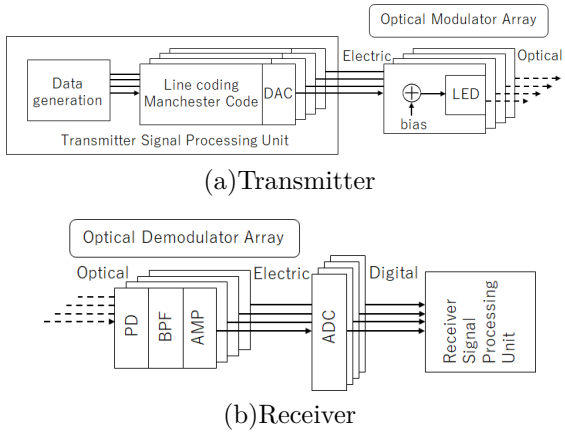

Fig. 2. Configuration of MIMO-OWC

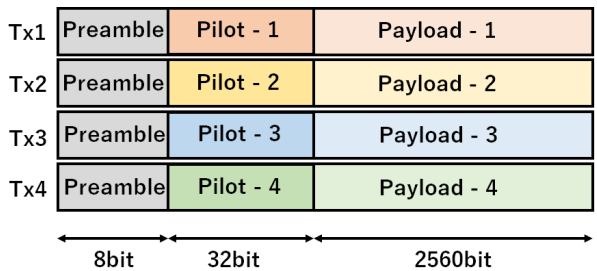

Fig. 3. Frame structure

Array" including four optical modulators. At the former unit, the digital data bit stream is first generated and then split into four parts to be structured into the corresponding frames. Afterward, the resulting frames are encoded using Manchester code, converted into electrical signals using a Digital Analog Converter (DAC), and output onto the optical modulators array. At the "Optical Modulator array" unit, the electrical signals are biased with a low direct current (DC) and finally modulated onto the LED.

2.1.1. Frame structure

As shown in Fig. 3, each data frame is composed of three parts, i.e., a preamble, a pilot, and a payload. Helping the receiver to easily identify the symbol position and determine the beginning of the frame, the preamble consists of an 8-bit sequence of alternating 1 and -1 bits, similar to each frame and given by

$$\boldsymbol{p} = [+1, -1, +1, -1, +1, -1, +1, -1] \tag{1}$$

For the pilot, it corresponds to the middle section of a data frame, including a 32-bit sequence. It is used to estimate the channel matrix at the receiver side. All the pilots are orthogonal to each other. For instance, the pilot data sequence $\mathbf{u_m}$ of the m-th frame can be expressed as follows.

$$\begin{aligned} \mathbf{u_1} &= [+\mathbf{e}, -\mathbf{e}, -\mathbf{e}, -\mathbf{e}], \mathbf{u_2} = [-\mathbf{e}, +\mathbf{e}, -\mathbf{e}, -\mathbf{e}] \\ \mathbf{u_3} &= [-\mathbf{e}, -\mathbf{e}, +\mathbf{e}, -\mathbf{e}], \mathbf{u_4} = [-\mathbf{e}, -\mathbf{e}, -\mathbf{e}, +\mathbf{e}] \end{aligned} \tag{2}$$

where,

$$\mathbf{e} = [1, 1, 1, 1, 1, 1, 1, 1] \tag{3}$$

Finally, each data frame ends with a payload including a sequence of 2560 bits.

2.1.2. Channel coding

The digital data frame is encoded by a widely used coding technique, i.e., Manchester coding at a symbol rate of $1/T_{Sym}$, and then conveyed to the optical modulator as an electrical signal by the DAC.

In fact, in this work, the Manchester coding technique was used in order to reduce the DC component as the amplifier of the optical modem incorporates a capacitive coupling that does not pass the DC component.

2.1.3. Optical modulator

In the "Optical Modulator Array" unit, the input electric signal of each optical modulator is firstly DC biased to ensure the constraint of the nonnegativity. Then, it modulates the intensity of the LED to generate an intensity-modulated optical signal to convey the information. All the four optical modulators have the same data rate.

2.2. Receiver

Fig.2 (b) illustrated the architecture of the MIMO-OWC receiver considered in this research. The receiver consists of three main parts, i.e., a receiving optical array unit including four optical demodulators, an Analog to Digital Converter (ADC), and a received signal processor unit. At first, the optical demodulator converts the received optical signal into an electrical one by eliminating the DC component. Afterward, the resulting signal is downsampled to generate a digital data stream by the ADC. At the received signal processor unit, the signal passes through a matched filter before being synchronized. After the estimation and equalization of the channel matrix, the transmitted signal can be finally recovered. In this work, the ADC output is stored and the signal processing is then performed offline. The different signal processes outlined above are detailed as follows.

2.2.1. Matched filter

After the conversion, the ADC digital output is filtered using a matched filter designed for Manchester coding. The output of the n-th optical demodulator of the MIMO-OWC receiver, is referred to as $r_n(t)$, and the corresponding ADC output is $r_n[l]$. Since the sampling is performed by the ADC at a period of T_{spl}, $r_n[l] = r_n(lT_{spl})$. In this experiment, we consider that $T_{Sym}/T_{spl} = 10$. The impulse response $h[i]$ of the filter that matches the transmission line code is given by

$$h[i] = \begin{cases} -1 & (0 \leq i \leq 4) \\ +1 & (4 < i \leq 9) \end{cases} \tag{4}$$

Hence, the matched filter output $r'_n[l]$ can be expressed as

$$r'_n[l] = \sum_{i=0}^{9} h[i] r_n[l-i] \tag{5}$$

2.2.2. Synchronization

During the synchronization process, the start of the frames, as well as the symbols timing are detected. In fact, we calculate the sum of the correlation of the matched filter output, $r'_n[l]$ and the preamble sequence, p, as expressed below. Then, the synchronization is performed by detecting the value of l which maximizes the sum.

$$\sum_{n=1}^{4} \sum_{i=0}^{7} (-1)^i r'_n[l + 10i] \tag{6}$$

After the symbol synchronization, the matched filter output $r'_n[l]$ is read every 10 samples and $q_n[k]$ is obtained and used for the following processing

$$q_n[k] = r'_n[10k + \Delta] \tag{7}$$

Note that Δ represents the amount of time shift during synchronization, and $q_n[0] = r'_n[\Delta]$ corresponds to the symbol at the beginning of the frame.

2.2.3. Channel matrix estimation

At the receiver, the channel matrix, H, where the m-th row and n-th column element $h_{n,m}$ represents the channel coefficient between the m-th optical modulator and the n-th optical demodulator can be estimated as follows

$$\widehat{\boldsymbol{H}} = \frac{1}{32} \begin{bmatrix} \boldsymbol{v_1} \\ \boldsymbol{v_2} \\ \boldsymbol{v_3} \\ \boldsymbol{v_4} \end{bmatrix} \begin{bmatrix} \mathbf{u_1}^T & \mathbf{u_2}^T & \mathbf{u_3}^T & \mathbf{u_4}^T \end{bmatrix} \tag{8}$$

where $\boldsymbol{v_n} = [q_n[8], q_n[9], \cdots q_n[39]]$ is the received symbol value corresponding to the channel estimate for the data sequence of the n-th optical demodulator output.

2.2.4. Equalization

After the channel matrix estimation, the zero-forcing technique is applied to equalize each symbol of the payload part. The estimated value $\widehat{x}_m[k]$ of the k-th symbol output corresponding to the m-th optical modulator can be expressed as

$$\begin{bmatrix} \widehat{x}_1[k] \\ \vdots \\ \widehat{x}_4[k] \end{bmatrix} = \widehat{\boldsymbol{H}}^{-1} \begin{bmatrix} \widehat{q}_1[k] \\ \vdots \\ \widehat{q}_4[k] \end{bmatrix} \tag{9}$$

Consequently, the estimated value $\widehat{d}_m[k]$ of the transmitted data is given by

$$\widehat{d}_m[k] = \mathrm{sgn}(\widehat{x}_m[k]) \tag{10}$$

3. Experimental environment and optical modem arrays calibration

In this section, the details of the experimental conditions in which we conducted our measurements are described. To evaluate the impact of the calibration on the overall system performance, the experiment was conducted twice, before and after applying a strict calibration. Table I outlines the specifications of the equipment used in the experiments.

3.1. Experimental environment

The experiments were performed at night, indoor, and in a static line-of-sight environment using infrared LEDs, emitting at a wavelength of 820 nm. The specifications of the experiments are summarized in Table II and the experimental setup is described in Fig. 4. The minimum distance separating the optical elements and the distance between the transmitting optical array and the receiving one correspond to d and L, respectively. In our experiment, we considered the same element spacing $d = 0.25$ m for both the linear and the square array arrangement of optical modems.

3.2. Calibration of transmitting and receiving optical arrays

Verification and selection of individual differences in modems

All the modems used in the experiments are commercial off-the-shelf optical modems that have been especially modified for our experiments. After the customization, these modems can transmit an

TABLE I
EXPERIMENTAL EQUIPMENT

Transmitter	
CPU	PXIe-8840
FPGA	PXIe-7972
DAC	PXIe-5783
Optical modulator	Toyo Electric SOT-ES200 (modified for experiments)

Receiver	
Optical demodulator	Toyo Electric SOT-ES200 (modified for experiments)
ADC	PXIe-5170
CPU	PXIe-8861

Optical modulator/demodulator	
LED	USHIO INK. HE8811
APD	Hamamatsu Photonics K.K. S12023-05
Wavelength	820 nm (IR)
Half-value angle	1°
3 dB Bandwidth	100 kHz - 40 MHz
Maximum gain frequency	500 kHz

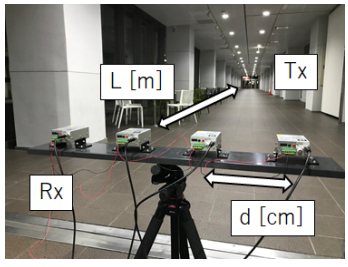

Fig. 4. Experimental test area

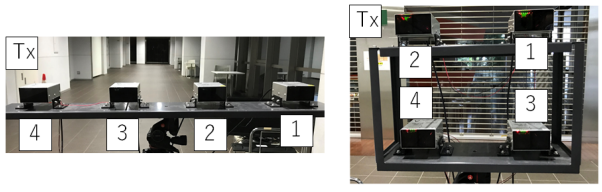

(a) (b)

Fig. 5. Position of optical modulators in the array for two different arrangements:(a) Linear arrangement (b) Square arrangement

arbitrary waveform. The letters "A" and "B" were initially used by the maker to differentiate between the two types of the optical modem before the modification. However, after the modification, all the modems have the same configuration.

In the first experiment, we did not take into consideration the characteristics of each optical modem included in the array, which affected conspicuously the results. Therefore, in the second experiment, before using them, we measured the transmission and reception performance of all the 18 optical modems we have. Optical modems are labeled from A1 to A9 and B1 to B9 and can be used as either an optical modulator or optical demodulator.

To measure the performance, a square wave with a voltage Vpp = 300 mV is input to the optical modulator. When measuring the reception performance of all optical modems A1 to A8 and B1 to B9, the modem labeled A9 is used as the optical modulator. On the other hand, when measuring the transmission performance of all the optical modems A1 to A9 and B1 to B8, the modem labeled B9 is used as the optical demodulator. In both measurements, the optical modulator and the optical demodulator were placed 15 cm apart, and an oscilloscope was used to measure the voltages.

Tables III and IV show the measurement results and the set of optical modems used in the experiments, respectively. The position of the optical modems within the array is described in Fig. 5. The individual differences seem to be due to manual customization done by the maker.

Angle calibration of optical modulator/demodulator in array

The transmitting and the receiving optical devices must be installed parallel to each other. Hence, at the transmitting side, we placed a screen in front of the optical modulators and adjusted their angle so that the projected infrared image had the same shape as the optical array. Afterward, we installed the receiving demodulator array at the screen position and adjusted the angle of each optical demodulator so that the output voltage was maximized. This adjustment was performed by placing a screen and a receiving array at a distance of 7 m from the transmitting array in the first

TABLE II
SPECIFICATIONS OF COMMUNICATION EXPERIMENT

Experiment environment	
Experimental location	Indoor (with background light)
MIMO size	4×4
Element spacing d	25 cm
Optical modem altitude	1.1 m
Communication distance L	Experiment 1 : 30,40,50,60,65 m
	Experiment 2 : 30,40,45,50,55,60,65 m
Signal parameters	
Modulation	Light intensity modulation
Transmission line code	Manchester code
Equalization method	zero forcing
symbol rate	25 Mbit/s ×4
ADC	
Bandwidth	100 MHz
Sampling rate	250 MSample/s

TABLE III
INDIVIDUAL PERFORMANCE OF OPTICAL MODEMS

Optical modem	Transmission	Reception
A1	252 mV	352 mV
A2	257 mV	301 mV
A3	220 mV	448 mV
A4	264 mV	264 mV
A5	155 mV	274 mV
A6	154 mV	226 mV
A7	216 mV	322 mV
A8	225 mV	292 mV
A9	289 mV	-

Optical modem	Transmission	Reception
B1	297 mV	435 mV
B2	291 mV	432 mV
B3	306 mV	424 mV
B4	322 mV	407 mV
B5	275 mV	290 mV
B6	290 mV	281 mV
B7	276 mV	288 mV
B8	296 mV	330 mV
B9	-	286 mV

experiment and 20 m in the second experiment.

Array position calibration

It is important that both the transmitting and the receiving optical arrays face each other accurately. Therefore, before conducting the experiment at each given distance, we adjusted the angle of the transmitter in order to capture the maximum of the incident light to the receiving elements. For this purpose, we used an infrared camera. After that, we adjusted the receiving optical demodulators so that the maximum output voltages could be achieved using an oscilloscope. For reference, Fig. 6 shows an infrared photograph of the transmitted light projected on the screen at each transmission distance.

4. Measurement results and discussion

The system performance is evaluated in terms of the channel matrix estimation and the measured BER of 4×4 optical MIMO while comparing both the newly proposed linear arrangement of optical

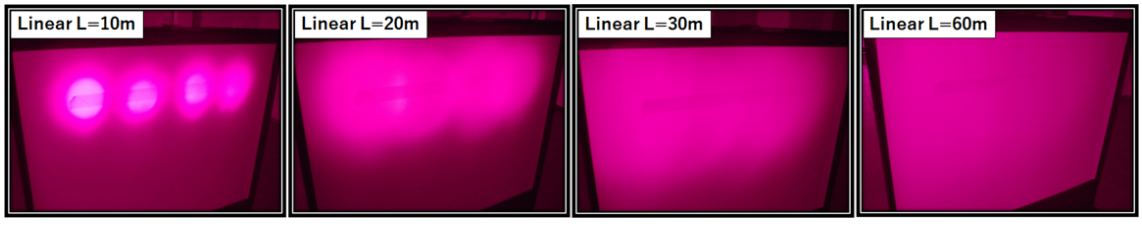

Fig. 6. State of projected transmitted light at each communication distance (infrared photograph)

TABLE IV
SELECTION TO ARRAY

(a) linear array

Position	Communication Experiment	
	First time	Second time
Tx1	A1	B4
Tx2	A2	B3
Tx3	A3	B2
Tx4	A4	B1
Rx1	B1	A5
Rx2	B2	A6
Rx3	B3	A7
Rx4	B4	A8

(b) square array

Position	Communication Experiment	
	First time	Second time
Tx1	A5	B6
Tx2	A6	B5
Tx3	A7	B8
Tx4	A8	B7
Rx1	B5	A2
Rx2	B6	A1
Rx3	B7	A3
Rx4	B8	A4

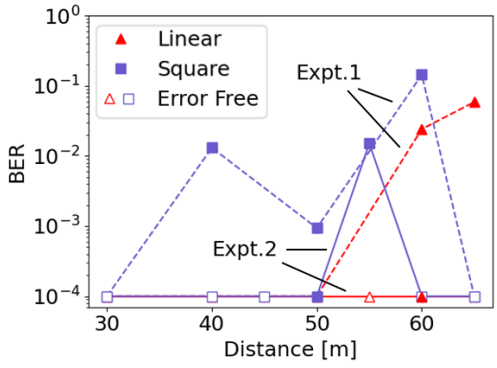

Fig. 7. Relationship between BER and communication distance (Experiments 1 and 2)

arrays and the conventional square arrangement of array elements

As described in Section 3, we conducted a first measurement experiment. Then, after performing a more strict calibration, and then conducted the measurement experiment again. In the following, we will refer to Experiment 1 and Experiment 2.

4.1. Relationship between BER and communication distance

Fig. 7 shows the relationship between the communication distance and BER. To determine the BER, we measured more than 50 frames (5×10^5 bits) of data at each measurement point. Except for the distance of 65 m, the system featuring the proposed linear arrangement of optical arrays achieves a better BER than the one using the conventional square constellation. However, in the case of the square array, it is still unclear why better results could be obtained at a distance of 65 m. Therefore, in order to improve the accuracy of the experiment, as explained in Subsection 3.2, in Experiment 2, a more strict calibration of the array element angle, and the array position by selecting the optical modem was applied as well. As a result, at a speed of 100 ($= 25 \times 4$) Mbps, we realized excellent characteristics of BER $< 10^{-4}$ in all cases except for the communication distance of 55 m with a square array arrangement. This high value of the BER was due to the imperfect calibration. In fact, it is more difficult to perform a strict calibration for the conventional square array. To the best of our knowledge, transmitting 100 Mbps over 65 m is considered as the highest data rate that could be achieved at the longest distance by indoor optical 4×4 MIMO system, using off-the-shelf LEDs and PDs. In the next section, we will confirm the obtained results while characterizing the channel matrix, with the purpose to evaluate the effects of the constellation of optical modems in more detail.

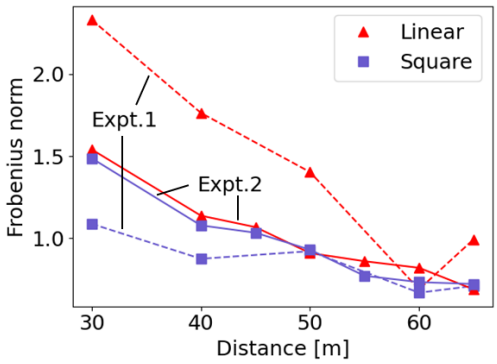

Fig. 8. Relationship between Frobenius norm and communication distance (Experiments 1 and 2)

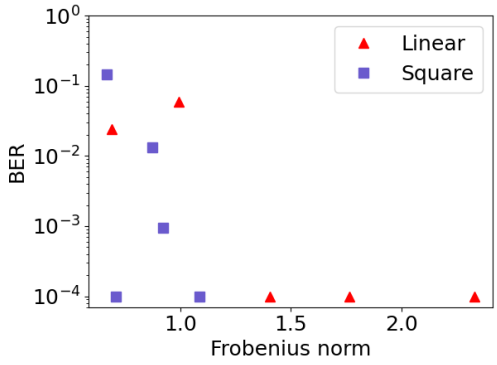

Fig. 9. Relationship between Frobenius norm and BER (Experiment 1)

4.2. Relationship between Frobenius norm and communication distance

Frobenius norm $||\widehat{H}||_F$ expressed by in Eq. (11) is one of the indexes showing the property of the estimated value of the channel matrix $\widehat{H}$.

$$||\widehat{H}||_F = \sqrt{\sum_{n=1}^{4}\sum_{m=1}^{4}\widehat{h}_{n,m}^2} \tag{11}$$

As clearly shown in its definition, the Frobenius norm is an index of the total received power of the receiving optical array when the transmitted optical power is constant. The relationship between the communication distance and the Frobenius norm in Experiments 1 and 2 is described in Fig. 8.

It can be seen that the total received power decreases with distance. In Experiment 1, the linear array has a larger Frobenius norm than the square array, which is considered to be largely affected by the individual differences of the elements described in Subsection 3.2. In Experiment 2, the difference between the two has almost disappeared.

4.3. Frobenius norm of channel matrix

The relationship between BER and the Frobenius norm in Experiment 1 is depicted in Fig. 9. In the region corresponding to $||H||_F \leq 1$, the BER differs greatly regardless of the value of the Frobenius norm, even if the total received power is the same, as seen in Fig. 9. This is thought to be related to

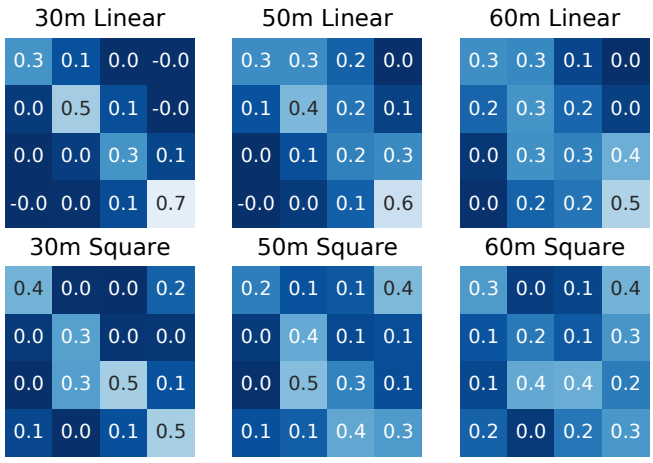

Fig. 10. Normalized estimated channel matrix $\widehat{H}/||\widehat{H}||_F$(Experiment 2)

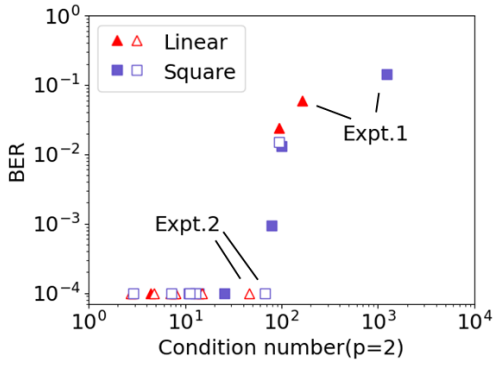

Fig. 11. Relationship between condition number and BER (Experiments 1 and 2)

the difference in the channel matrix. Fig. 10 illustrates the normalized estimated matrix $\widehat{H}/||\widehat{H}||_F$. For a short transmission distance of 30 m, only the value of the diagonal component in the channel matrix is large (i.e., the communication between the opposing elements is dominant), whereas for a longer distance of 60 m, the values of the other components are also large. It is clear that as the distance increases, the size of the off-diagonal components cannot be ignored, and it changes in a complicated manner depending on the distance and the type of the array arrangement.

4.4. Condition number of channel matrix

To characterize the changes in the transmission channel matrix, we considered the condition number κ expressed as

$$\kappa_2(\widehat{H}) = ||\widehat{H}||_2 \cdot ||\widehat{H}^{-1}||_2 = \frac{\sigma_{\max}(\widehat{H})}{\sigma_{\min}(\widehat{H})} \tag{12}$$

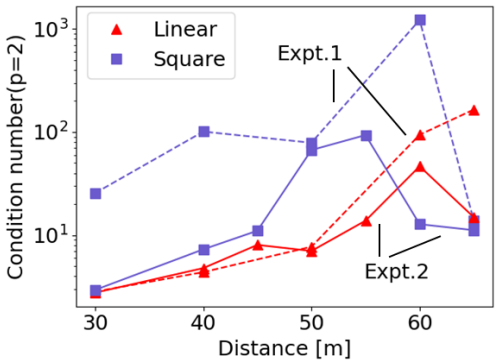

Fig. 12. Relationship between the condition number and communication distance (Experiments 1 and 2)

where $\sigma_{\max}(\widehat{H})$ and $\sigma_{\min}(\widehat{H})$ indicate the maximum and minimum singular values of $\widehat{H}$. By definition, the condition number is an index of the impact of the initial error on the solution of simultaneous linear equations expressed by a matrix. In this study, it characterizes the effect of the noise on the results of the zero-forcing equalization.

As shown in Figure 11, a larger condition number is obtained in the case of Experiment 1 rather than Experiment 2. This highlights the fact that the effect of the initial error is much more significant in Experiment 1 [1].

4.5. Relationship between the condition number and communication distance

Figure 12 depicts the condition number of the estimated channel matrix at each distance up to 65 m. It is clear that the condition number increases with the transmission distance. Moreover, in Experiment 2, smaller condition numbers are obtained. This shows the importance of conducting a strict calibration. By comparing both constellations of optical modems, we can see that the conventional square array has a larger variation in terms of the condition number, showing to be more sensitive to the installation errors. In fact, in the case of the proposed linear arrays, the parallelism of one-dimensional line segments should be parallel, whereas, for the square constellation, parallelism is required in the two-dimensional planes.

5. Conclusion

In this research work, we experimentally evaluated the performance of a newly designed 4×4 MIMO-OWC system featuring a horizontal linear constellations of optical modems, for high data rate transmission over long-range distances. To characterize the dependence of the transmission channel matrix into the selection of the arrangement of optical elements, we elaborate on a comparative performance study in terms of both the channel matrix estimation and the measured BER up to a distance of 65 m. For this purpose, two important metrics of the MIMO transmission channel matrix are considered, namely the Frobenius norm and the condition number. Based on the obtained results, the BER is dominated by the channel matrix shape expressed by the condition number, in the case of Frobenius norm values not exceeding 1. Furthermore, we also assessed the impact of the calibration on the performance of the MIMO-OWC system for both constellations. It is shown that the conventional optical system using square arrays is much more susceptible to the calibration error rather than the newly proposed linear arrangement of optical arrays. The obtained results show that our system can achieve high performance with relatively low directivity that relaxes the

[1]From the viewpoint of the channel capacity when an error correction code is applied, the condition number is not always a good index for MIMO systems with 3 or more elements [18].

requirements in terms of calibration accuracy. Thanks to the ease of implementation and calibration, the linear array is more advantageous than other possible configurations. There is room for more detailed theoretical discussion on the optimum arrangement as well as the optimized separation between the optical modems for a given communication distance.

Acknowledgements

We are deeply grateful to Professor Takaya YAMAZATO, Nagoya University, for his guidance and encouragement in carrying out this research. We would also like to thank the Toyo Electric Corporation for their technical support, especially for the customization of the optical modems. This work was supported by JSPS Grants-in-Aid for Scientific Research 17H03265.

References

[1] Ministry of Education, Culture, Sports, Science and Technology (MEXT), Japan, "Chapter 2 The Direction of Japans efforts towards realizing a super smart society (Society 5.0)," in White Paper on Science and Technology 2016, pp. 97-179, 2016.
[2] P. W. Berenguer, D. Schulz, J. Hilt, P. Hellwig, G. Kleinpeter, J.K. Fischer, "Optical wireless MIMO experiments in an industrial environment," IEEE J. Select. Areas, vol.36, no.1, pp. 185-193, 2018.
[3] B. Holfeld *et al.*, "Wireless communication for factory automation: An opportunity for LTE and 5G systems, IEEE Commun. Mag., vol.54, no.6, pp.36-43, 2016.
[4] S. A. Ashraf *et al.*, Ultra-reliable and low-latency communication for wireless factory automation: From LTE to 5G, in 2016 IEEE 21st International Conference on Emerging Technologies and Factory Automation (ETFA), Berlin, Sep. 2016.
[5] A. Paraskevopoulos et al., Optical Wireless Communication Systems in the Mb/s to Gb/s Range, Suitable for Industrial Applications, IEEE/ASME Trans. Mechatron., vol.15, no.4, pp.541547, Aug. 2010.
[6] Y. Wang, X. Huang, L. Tao, J. Shi, and N. Chi, "4.5-Gb/s RGB-LED based WDM visible light communication system employing CAP modulation and RLS based adaptive equalization," Optics Express, vol.23, no.10, pp.13626-13633, 2015.
[7] H. Chun et al., "LED based wavelength division multiplexed 10 Gb/s visible light communications," J. Lightw. Technol., vol.34, no.13, pp. 3047-3052, 2016.
[8] E. Xie et al., "Over 10 Gbps VLC for Long-Distance Applications Using a GaN-Based Series-Biased Micro-LED Array," IEEE Photon. Technol. Lett., vol.32, no.9, pp. 499-502, May 2020.
[9] Y. Wang, N. chi, "Demonstration of High-Speed 2 × 2 Non-imaging MIMO Nyquist single carrier visible light communication with frequency domain equalization," J. Lightw. Technol., vol.32, no.11, pp.2087-2093, 2014.
[10] C. Hsu, C. Chow, I. Lu, Y. Liu, C. Yeh, Y. Liu, "High speed imaging 3 × 3 MIMO Phosphor white LED based visible light communication system," IEEE Photon. J., vol.8, no.6, 2016.
[11] L. Wei, H. Zhang, J. Song, "Experimental demonstration of a cubic-receiver-based MIMO visible light communication system," IEEE Photon. J., vol.9, no.1, 2016.
[12] A. Burton, H.L. Minh, Z. Ghassemlooy, E. Bentley, C. Botella, "Experimental demonstration of 50-Mb/s visible light communications using 4 × 4 MIMO," IEEE Photonics Technology Letters, vol 26, no.9, pp.945-948, 2014.
[13] F. Corona, H. Sugiura, K. Kobayashi, H. Okada, M.Katayama, "Experimental evaluation of an optical wireless MIMO system with baseband modulation," IEICE Technical Report, RCS2018-115, vol.118, no.125, pp.165-169, 2018.
[14] T.Nakamura, K. Kobayashi, H. Okada, M.Katayama, "Experimental evaluation on communication distance of an optical wireless MIMO system using linear arrays," IEICE General Conference, no.A-9-22, p.101, Mar. 2020.
[15] D. Takase and T. Ohtsuki, "Performance analysis of optical wireless MIMO with optical beat interference," in Proc. of the IEEE International Conf. on Commun., Korea, pp. 954958, May 2005.
[16] D. Takase and T. Ohtsuki, "Spatial multiplexing in optical wireless MIMO communications over indoor environment," IEICE Trans. Commun., vol.E89B, no.4, pp. 1364-1371, 2006.
[17] H. Sugiura, K. Kobayashi, H. Okada, M.Katayama, "Experimental evaluation of element spacing in indoor optical wireless MIMO systems," IEICE Technical Report, WBS2017-32, pp.51-55, Oct. 2017.
[18] H. Sugiura, K. Kobayashi, H. Okada, M.Katayama, "A study on the relationship between channel matrices and communication performance in indoor optical wireless MIMO systems," IEICE Technical Report, WBS2018-35, pp.47-52, Dec. 2018.